JVST B
Journal of Vacuum Science & Technology B

ARTICLE

pubs.aip.org/avs/jvb

Study of the UHV compatibility of selected ferritic stainless steels for application in vacuum systems of future gravitational wave detectors

Cite as: J. Vac. Sci. Technol. B 43, 044203 (2025); doi: 10.1116/6.0004698
Submitted: 6 May 2025 · Accepted: 11 June 2025 ·
Published Online: 11 July 2025

View Online Export Citation CrossMark

Carlo Scarcia,[a] Giuseppe Bregliozzi, Paolo Chiggiato, and Ivo Wevers

AFFILIATIONS

CERN, 1211 Geneva 23, Switzerland

[a]**Author to whom correspondence should be addressed:** carlo.scarcia@cern.ch

ABSTRACT

Future gravitational wave detectors (GWDs), such as the Cosmic Explorer and the Einstein Telescope, demand extensive ultrahigh vacuum (UHV) systems, making material cost and performance critical considerations. This study explores the potential of ferritic stainless steel, specifically AISI 441 and AISI 444, as a cost-effective alternative to the commonly used austenitic stainless steel for UHV components, focusing on the analysis of outgassing rates pre- and postbakeout at 80 and 150 °C for 48 h. With hydrogen contents up to 50 times lower than those measured in standard AISI 304L steel, the tested grades showed, after bakeout, hydrogen outgassing rates down to 10^{-15} mbar l s^{-1} cm^{-2}. The measured values are three orders of magnitude lower than those of similarly conditioned austenitic stainless steels. These results highlight ferritic stainless steel as a promising, economical, and high-performance candidate for future GWDs vacuum systems.

I. INTRODUCTION

The direct detection of gravitational waves in 2015[1] opened a new way to observe the universe and revolutionized astrophysics, marking a significant advancement in our understanding of the cosmos. The ultrasensitive laser interferometry employed in the gravitational wave detectors (GWDs) is used to measure the space-time deformation attenuating all noise sources[2] that might hinder the measurements.

One of the sources of noise originates from the residual gas molecules present along the laser paths, which can extend for several kilometers. To minimize the scattering of photons caused by random fluctuations of gas molecules within the volume through which the laser travels, the laser paths must operate in an ultrahigh vacuum (UHV) environment. This reduces variations in the refractive index and associated phase shifts experienced by the photons.[3] Typically, the UHV requirements are designed to guarantee a residual gas noise along the interferometer's arms equivalent to 10% of the sum of all the other noises (thermal, seismic, quantum, etc.).

The current generation of GWDs [such as LIGO (Ref. 4), Virgo (Ref. 5), and KAGRA (Ref. 6)] has marked the 200th detection during the last operational run,[7] and they continue to serve as a valuable source of insights through ongoing improvements. However, their performance remains limited, as in a couple of decades they will reach their ultimate sensitivity.

To broaden the scope of potential discoveries, a third generation of gravitational wave detectors (3G-GWDs) is being developed, in particular, the Cosmic Explorer (CE) in the United States and the Einstein Telescope (ET) in Europe. The CE design, resembling that of LIGO, will be composed of two 90° angled interferometers hosted in two different locations with arm lengths of 40 km. CE will require about 160 km of vacuum beam pipes with an inner diameter of 1.2 m.[8] ET, instead, will consist of six interferometers arranged in an equilateral triangle in an underground tunnel with 10 km sides. This layout will require, per tunnel, four UHV beam pipes arranged in two vertically stacked pairs. The beam pipes will have an internal diameter of 1 m and develop for a total length of 120 km.[9]

The considerable size of beam pipe vacuum systems could significantly impact the overall experiment cost, motivating the need for improved designs, manufacturing techniques, and materials relative to the current generation of GWDs.[10] Therefore, it is essential

to select materials and fabrication processes that ensure UHV performance and optimize costs with respect to the high-temperature treated 304L currently used in gravitational wave observatories.[11]

In a recent study, we explored the UHV compatibility of mild steels as a potential alternative to austenitic stainless steel for the fabrication of UHV-compatible beam pipes.[12] The findings revealed that the tested mild steels exhibited remarkably low outgassing rates, outperforming by several orders of magnitude standard UHV-compatible austenitic stainless steels that are not vacuum or air fired. However, despite its lower raw material cost and demonstrated UHV compatibility, concerns remained regarding its susceptibility to internal surface changes and limited corrosion resistance. Addressing these issues may require additional treatments or coatings, which could diminish the mild steel's overall cost advantage.

Another alternative candidate to substitute the austenitic stainless steel currently used for GWDs could be ferritic stainless steel. Characterized by a fully ferritic microstructure at room temperature, these stainless steels are not commonly used in accelerators and surface science equipment due to their soft magnetic properties[13] and rapid ductile-to-brittle transition below room temperature, which hinders their use in cryogenic applications as well.[14] Indeed, the few studies of a UHV application of ferritic stainless steel involved shielding a particle beam from an external magnetic field. The authors of the study report a hydrogen content of 0.04 ppm weight in AISI 430, a ferritic stainless steel grade used to produce ISO flanges.[15] The content, extracted via temperature programed desorption (TPD) measurements, was found to be 12 times lower than that in AISI 316L. In a related study, the water outgassing rate after 100 h of pumping for AISI 430 was found to be similar to that of AISI 304.[16] Unfortunately, these studies did not directly measure the hydrogen outgassing rate. If these rates are as low as those reported for mild steels, ferritic stainless steels will offer the same benefits as mild steel while also addressing the corrosion problems associated with low-carbon structural steels.

Building upon our earlier work, this study evaluates ferritic stainless steel as a potential material for 3G-GWDs vacuum beam pipes. We measured the outgassing rates of alloyed ferritic stainless steel grades, focusing on H_2, H_2O, CH_4, CO, and CO_2 commonly found in the UHV regime. We utilized commercially available products to ensure cost-effectiveness and measured a low-temperature bakeout impact on outgassing rates. Alongside the outgassing measurements after bakeout, we assessed the diffusable H_2 content within the tested alloys via TPD measurements.

II. EXPERIMENTAL APPARATUS AND METHODS

A detailed description of the experimental apparatus and measurement steps can be found elsewhere.[12] Below, we report the relevant information and changes to the systems used for this study.

A. Throughput method

The outgassing rate of unbaked samples was measured via the throughput method.[17–19] Pumping speed was provided through an orifice with a diameter of 0.8 cm, which results in conductance for water vapor of $C_{H_2O} = 7.4\,l\,s^{-1}$. The evolution of the specific outgassing rate was measured for approximately 100 h of pumping, with the room temperature stabilized at $21 \pm 2\,^{\circ}C$. To ensure the measurement's reproducibility, the background contribution was remeasured every time a new grade was tested.

B. Coupled accumulation-throughput method

The postbakeout outgassing rates of the samples were measured using the coupled accumulation-throughput method.[18,19] The samples were baked at 80 and 150 °C for 48 h, while the rest of the system was baked at temperatures up to 350 °C. The accumulation measurements were performed at room temperature ($21 \pm 2\,^{\circ}C$), at least 24 h after the samples reached room temperature at the end of the bakeout. For all the tested alloys, the linearity between accumulated partial pressures of the gases and time has been verified by repeating the measurements for different accumulation times.

C. Temperature programed desorption

The diffusible hydrogen content within the selected steels was determined with TPD measurements. The TPD analyses were performed using a commercial TPD workstation.[20] The samples, each measuring 1×1 cm and varying in thickness from 0.15 to 0.3 cm, were heated from 25 to 940 °C with a ramp rate of 5 K/min. The background was remeasured after every ten samples to ensure measurement reproducibility. The calculation of the hydrogen concentration was based on sample weight, measured with a scale with a sensitivity of ± 0.1 mg.

III. MATERIAL SELECTION AND SAMPLE PREPARATION

AISI 441 and AISI 444 off-the-shelf sheets were acquired from the market and compared with AISI 304L sheets from the CERN supply and specific for UHV applications. The chemical and forming characteristics of the selected steels are listed in Table I. The samples for the UHV characterization were extracted from the sheets by dry cutting them to the required dimensions using a bench shear. Both the ferritic grades and the AISI 304L samples were cleaned following the CERN UHV standard procedure[21] consisting of an alkaline detergent bath, rinsing with demineralized water, and drying in an air furnace.

IV. RESULTS AND DISCUSSION

A. Water vapor outgassing rate

The pumpdown curves, representative of the water vapor specific outgassing rate as a function of pumping time, are shown in Fig. 1. The specific outgassing rates recorded at 10 h of pumping are reported in Table II.

As shown in Fig. 1, the pumpdown curves of the selected grades are fitted fairly well by the inverse law of pumping time with the empirical law (dashed line) $q_{H_2O} = \frac{3\times10^{-9}}{t[h]}\,mbar\,l\,s^{-1}\,cm^{-2}$.[18] The observed behavior is in line with that of metal surfaces discussed and interpreted by some authors.[23–25] Quantitatively, both ferritic grades tested align with the values of AISI 304L, with the AISI 444 measuring the lowest outgassing rate after 10 h of pumping of $2.4 \times 10^{-10}\,mbar\,l\,s^{-1}\,cm^{-2}$. The differences observed in the water vapor outgassing rate values could be due to the

TABLE I. Chemical composition in wt. % of the tested alloys with additional information on the forming process, heat treatment, surface finish, shape, and thickness tested. The reported AISI 304L chemical composition is to be intended as the maximum content allowed (Ref. 22). CR, cold rolled; HR, hot rolled; RA, recrystallization annealed; and SA, solution annealed.

	AISI 441	AISI 441	AISI 444	AISI 304L
Forming process	CR	HR	CR	CR
Heat treatment	RA	RA	RA	SA
Surface finish	2B	2D	2D	2D
Shape	Sheet	Sheet	Sheet	Sheet
Thickness (cm)	0.15	0.3	0.15	0.15
C	0.015		0.011	0.03
Mn	0.385		0.3	2.0
Si	0.584		0.38	1.0
S	0.001		0.0014	—
P	0.0029		0.0029	0.03
N	0.014		0.016	0.02
Cr	17.57		18.89	17–20
Ni	0.242		—	10–12.5
Mo	—		1.892	—
Ti	0.16		0.006	—
Nb	0.4		0.566	—
Fe	Remainder		Remainder	Remainder

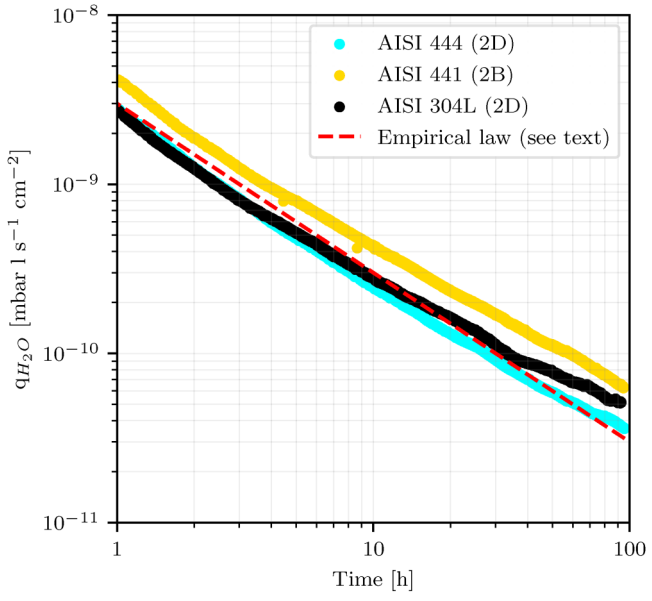

FIG. 1. Pumpdown curves measured at 21 ± 2 °C; the specific outgassing rate is plotted as a function of the pumping time. The background value is subtracted. The empirical law, calculated as reported in the text, is generally applied at CERN for UHV-compatible austenitic stainless steels. In parentheses, the surface finish of the tested alloys.

TABLE II. Water vapor specific outgassing rates measured at 21 ± 2 °C at 10 h of pumping. Background removed.

Grade	Surface tested (cm^2)	$q_{10\,h}$ (mbar l s^{-1} cm^{-2})
AISI 441	4630	4.3×10^{-10}
AISI 444	9260	2.4×10^{-10}
AISI 304L	5956	3.3×10^{-10}

different roughness of the tested specimens rather than attributable to the grades.

B. Temperature programed desorption

The H_2 thermal desorption mass spectra are shown in Fig. 2. For better visualization, the raw data were smoothed through a Savitzky–Golay filter.[26]

As shown in Fig. 2, the spectra of AISI 304L samples report a broad peak with a maximum at 480 °C. The signal can be fitted by a Fickian diffusion model with a diffusion energy of 0.52 ± 0.06 eV, a typical value in austenitic stainless steels.[27–29]

The H_2 spectra of the two ferritic stainless steels show similar features (see Fig. 3). The AISI 441 samples are characterized by a narrow peak around 250–260 °C, followed by a shoulder at 420 °C. Additionally, the spectra feature a broad peak or shoulder between 530 and 750 °C before ramping up. Similarly, the AISI 444 samples exhibit the same peaks and shoulders, although the initial and highest peak is shifted to 420 °C.

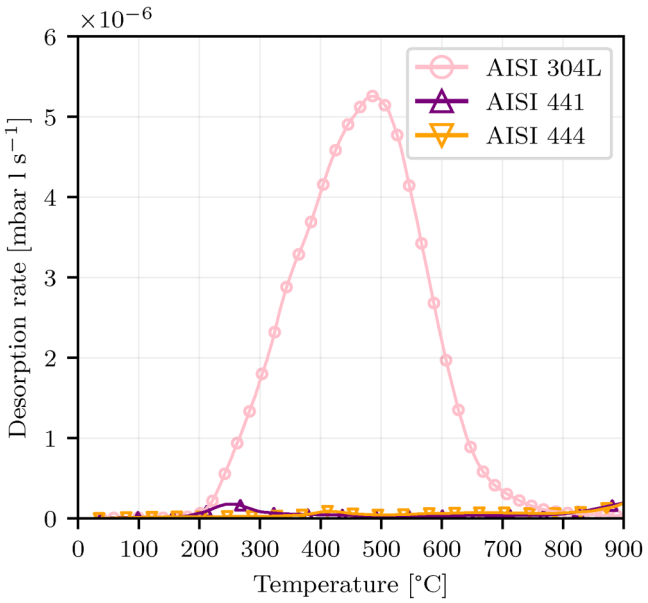

FIG. 2. H_2 TPD spectra of AISI 304L, AISI 441, and AISI 444 0.15 cm thick samples. The contribution of the TPD system is removed. Heating rate: 5 K/min.

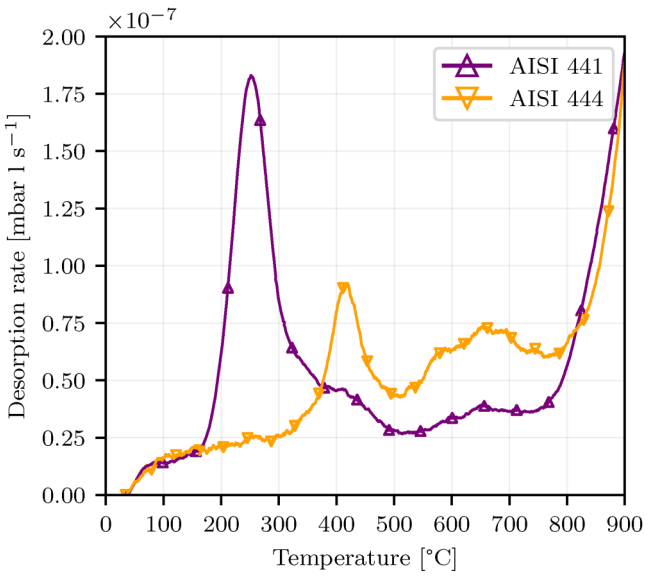

FIG. 3. H_2 TPD spectra of AISI 441 and AISI 444 samples (vertical scale reduced 30× with respect to Fig. 2). The contribution of the TPD system is removed. Heating rate: 5 K/min.

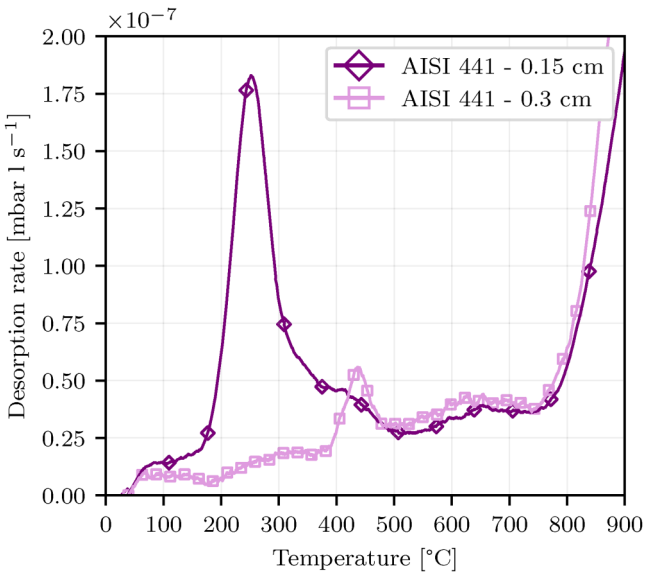

FIG. 4. H_2 TPD spectra of AISI 441 0.15 and 0.3 cm thick samples. The former were skin passed while the latter were not. Heating rate: 5 K/min.

The shape of the peaks defining the ferritic stainless steel's H_2 TPD spectra appears not to follow Fickian desorption but rather influenced by H detrapping from specific energy sites (grain boundaries, inclusions, etc.).[30–32]

The high-intensity peak observed in the AISI 441 samples may be attributed to the production process of the raw materials. The residual dislocations from cold rolling in the AISI 441 samples could be accentuated by the subsequent skin passing required to achieve the 2B finish. In contrast, the AISI 444 samples, which were provided with a 2D finish and were not subjected to skin passing, did not exhibit this peak.

To further support the detrapping-limited H_2 desorption and the effect of the production processes, 0.3 cm thick hot-rolled AISI 441 samples were tested. The 0.3 cm samples had similar chemical composition and the same 2B surface finish as the 0.15 cm ones.

As depicted in Fig. 4, the 0.3 cm samples did not show the first main peak at around 250 °C but rather a lower intensity at around 430 °C, similar to what was observed for the AISI 444 samples. Therefore, the results seem to confirm the proposed interpretation of the data reported in Fig. 3.

It is important to note that if we exclude the main peak around 250 °C for the 0.15 cm thick AISI 441 samples, the position of the main peak appears to remain invariant regardless of the thickness and grade of the tested ferritic stainless steel.

The H_2 concentration in the samples is calculated by arbitrarily integrating the TPD signal up to 850 °C, assuming a uniform initial distribution throughout the sample volume. The upper limit of the integration range is supported by the observation that hydrogen released above 850 °C is considered tightly bound and, therefore, nondiffusible within the temperature range experienced in most UHV applications. The calculation results are reported in Table III.

The hydrogen concentration in AISI 304L samples is 41–53 times higher than that extracted from the ferritic stainless steel samples, the latter desorbing H contents always below 2 atomic ppm. This outcome was foreseeable due to the ferritic specimens' body-centered-cubic (BCC) structure, which has much lower hydrogen solubility than the austenitic face-centered-cubic microstructure of AISI 304L.

C. Postbakeout outgassing rates

As shown in Table IV, the selected ferritic grades showed exceptionally low outgassing rates after an 80 °C 48 h long bakeout. The AISI 444 specimens had an H_2 specific outgassing rate of 1×10^{-15} mbar l s^{-1} cm^{-2}, and for CH_4, CO, and CO_2 values ranging between 1.8×10^{-16} and 6.1×10^{-16} mbar l s^{-1} cm^{-2}. In contrast, the AISI 441 samples showed a CH_4 specific outgassing rate of 1.1×10^{-16} mbar l s^{-1} cm^{-2}, while the H_2, CO, and CO_2 outgassing rates fell below the system sensitivity, arbitrary set as 50% of the background value.

TABLE III. AISI 444, AISI 441, and AISI 304L hydrogen concentration. The values are the average of at least three samples. The background of the TPD system is removed. The AISI 304L samples are not vacuum fired.

Grade	H content (ppm at.)	Thickness (cm)
AISI 304L	70	0.15
AISI 441	1.7	0.15
AISI 444	1.3	0.15

TABLE IV. Room temperature (21 ± 2 °C) specific outgassing rates of the selected stainless steels after bakeout at 80 °C for 48 h. Background removed. BSS, below system sensitivity.

	Specific outgassing rate (mbar l s^{-1} cm^{-2})			
Grade	H_2	CH_4	CO	CO_2
AISI 441	BSS	1.1×10^{-16}	BSS	BSS
AISI 444	1.0×10^{-15}	6.1×10^{-16}	4.1×10^{-16}	1.8×10^{-16}
AISI 304L	7.2×10^{-13}	1.1×10^{-15}	2.2×10^{-15}	3.4×10^{-16}

After the following bakeout at 150 °C for 48 h (see Table V), the specific outgassing rates of AISI 441 fell below the system sensitivity, except for CH_4, which decreased by approximately a decade. For the AISI 444 samples, besides the H_2 outgassing rate being shadowed by the background value, CH_4, CO, and CO_2 showed reductions in outgassing by factors of 1.4–20 compared to the 80 °C bakeout (Figs. 6–8).

Compared to the similarly tested 304L samples, the selected ferritic alloys report H_2 specific outgassing rates from two to four orders of magnitude lower if considering the system sensitivity, therefore attaining values comparable if not lower than similar thickness austenitic stainless steel after vacuum firing[18] or air bakeout.[33]

Similarly to what was observed for mild steel[12] in a previous study, the ratios of hydrogen concentration and specific hydrogen outgassing rates for the ferritic grades, compared to austenitic steels, do not align quantitatively. As hinted by the TPD spectra discussed above, the hydrogen may be trapped in different low-energy sites; thus, desorption is not limited by diffusion at room temperature. It is worth noting the increase in the H_2 outgassing rate observed for AISI 304L when baked out at 80 and 150 °C. An analogous behavior is evident in the background of these measurements (see Fig. 5) and in line with observations reported by previous studies focused on vacuum fired austenitic stainless steels.[34] However, the increase in the outgassing rate observed here for untreated 304L samples was significantly higher than what was previously reported for vacuum fired specimens. This trend, which might be relevant to the considered application, will be investigated in future work.

TABLE V. Room temperature (21 ± 2 °C) specific outgassing rates of the selected stainless steels after bakeout at 150 °C for 48 h. Background removed. BSS, below system sensitivity.

	Specific outgassing rate (mbar l s^{-1} cm^{-2})			
Grade	H_2	CH_4	CO	CO_2
AISI 441	BSS	1.0×10^{-17}	BSS	BSS
AISI 444	BSS	4.3×10^{-16}	9.1×10^{-17}	8.8×10^{-18}
AISI 304L	7.5×10^{-12}	3.7×10^{-15}	6.7×10^{-15}	BSS

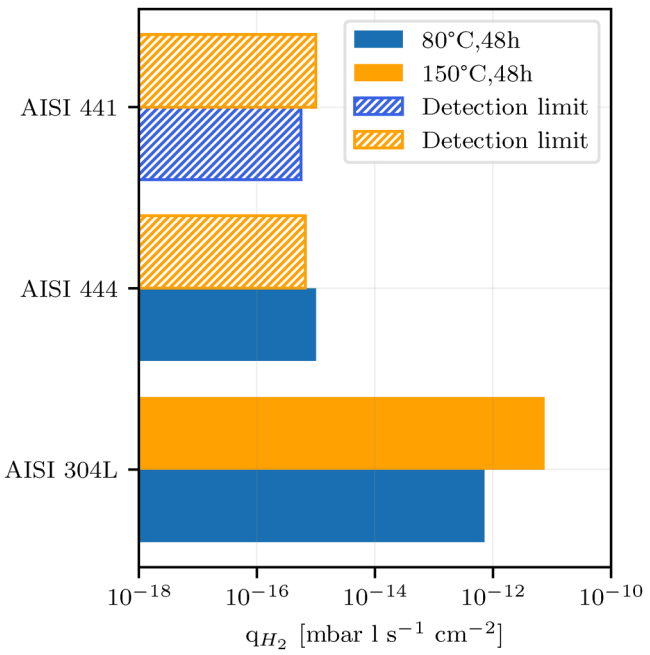

FIG. 5. Visualization of H_2 specific outgassing rate reported in Tables IV and V. The dashed columns indicate measurements below the detection limit and represent the system sensitivity normalized to the sample surface area.

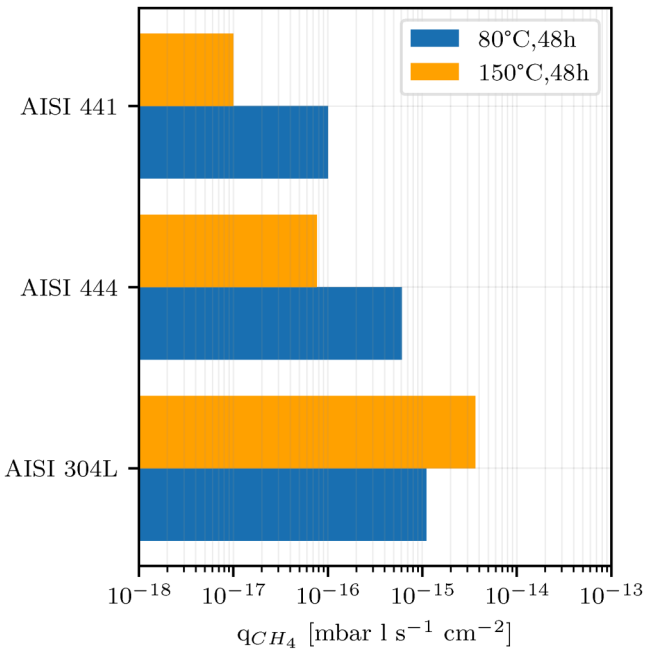

FIG. 6. Visualization of CH_4 specific outgassing rate reported in Tables IV and V.

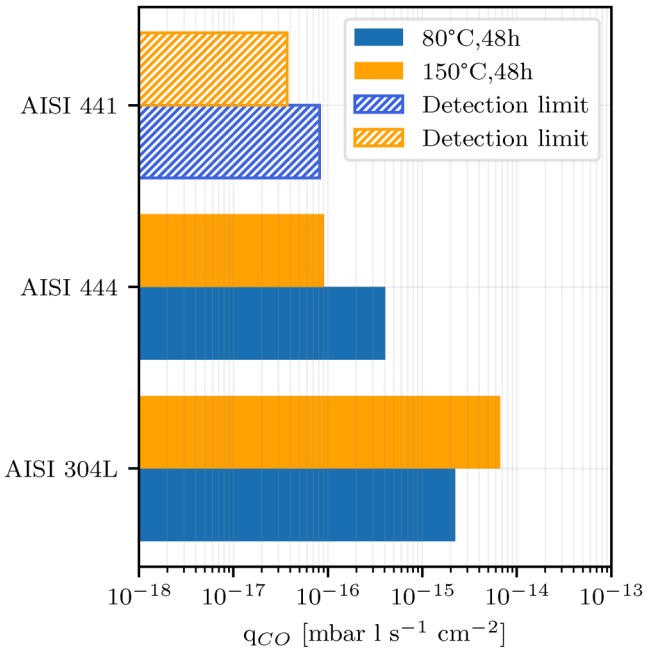

FIG. 7. Visualization of CO specific outgassing rate reported in Tables IV and V. The dashed columns indicate measurements below the detection limit and represent the system sensitivity normalized to the sample surface area.

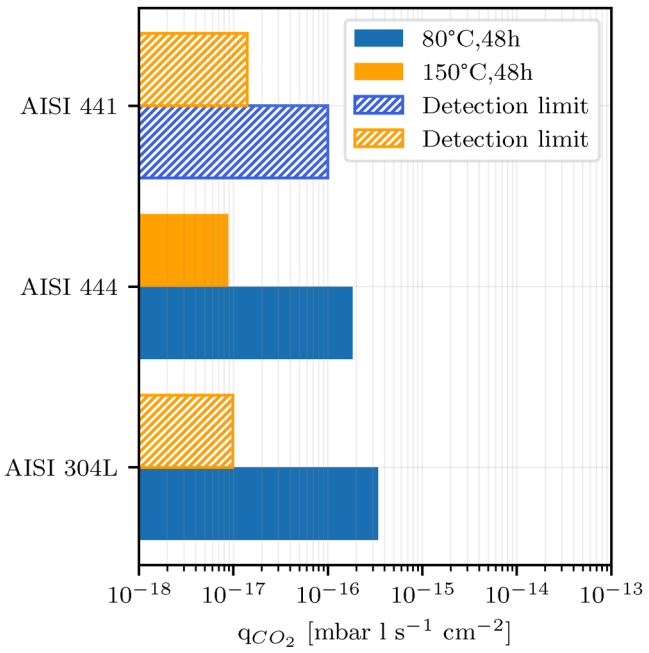

FIG. 8. Visualization of CO_2 specific outgassing rate reported in Tables IV and V. The dashed columns indicate measurements below the detection limit and represent the system sensitivity normalized to the sample surface area.

V. CONCLUSIONS

In this work, we investigated the UHV compatibility of ferritic stainless steels for the construction of vacuum beam pipes of next-generation GWDs.

The water vapor outgassing rate of the selected ferritic stainless steels obeys the typical reciprocal function of the pumping time, showing values in line with those measured for austenitic stainless steels. Differences are considered to be more related to different surface roughness than to the grades of the steel.

The TPD analysis demonstrated that the ferritic stainless steel samples have a remarkably lower hydrogen content, ranging from 41 to 53 times less, than in as-cleaned AISI 304L. This difference was expected due to the lower hydrogen solubility of the BCC structure that characterizes the ferritic alloys. The H_2 TPD spectra indicate a more complex desorption process than austenitic stainless steel's typical Fickian diffusion profile. The shape and position of the desorption peaks indicate a detrapping-limited mechanism. In support of this hypothesis, an invariance in peak position has been observed when testing different thicknesses and surface finishes of the same grade.

The H_2 specific outgassing rates, measured at room temperature after an 80 °C 48 h bakeout, lie within the range of 10^{-15} mbar l s^{-1} cm^{-2}, in line with those observed for austenitic stainless steels after extensive heat treatments like the vacuum firing or the air bakeout. The recorded outgassing values in the as-cleaned state for the selected ferritic stainless steels meet the low outgassing requirements for future gravitational wave detectors, therefore avoiding costly and extensive degassing treatments.

While ferritic stainless steels offer an economical and high-performing alternative to austenitic stainless steels for UHV compatibility, positioning them as a promising baseline material for 3G GWDs vacuum pipes construction,[35] their applicability from a manufacturing perspective is not yet fully established.

A potential grain growth in the heat affected zone of the weld line in ferritic stainless steels can lead to reduced mechanical strength in the welded area. This issue can be addressed by selecting stabilized ferritic stainless steel grades, such as AISI 441 or AISI 444, which contain titanium and niobium to limit grain growth during cooling. Additionally, careful optimization of welding parameters can help mitigate this effect. These considerations, along with a quantitative evaluation of corrosion resistance, are the focus of ongoing studies before ferritic stainless steels can be definitively established as the new baseline material for UHV beampipes in 3G GWDs.

ACKNOWLEDGMENTS

We thank Alice Michet and Jonathan Gaudio for their contribution to the outgassing measurements. This work has been sponsored by the Wolfgang Gentner Programme of the German Federal Ministry of Education and Research (Grant No. 13E18CHA).

AUTHOR DECLARATIONS

Conflict of Interest

The authors have no conflicts to disclose.

Author Contributions

Carlo Scarcia: Conceptualization (lead); Data curation (lead); Investigation (lead); Methodology (equal); Validation (lead); Visualization (lead); Writing – original draft (lead). **Giuseppe Bregliozzi:** Methodology (equal); Supervision (lead); Writing – review & editing (lead). **Paolo Chiggiato:** Resources (equal); Supervision (equal); Writing – review & editing (equal). **Ivo Wevers:** Conceptualization (equal); Investigation (equal); Supervision (equal); Writing – review & editing (equal).

DATA AVAILABILITY

The data that support the findings of this study are available from the corresponding author upon reasonable request.

REFERENCES

[1]B. P. Abbott *et al.*, Phys. Rev. Lett. **116**, 061102 (2016).
[2]D. V. Martynov *et al.*, Phys. Rev. D **93**, 112004 (2016).
[3]M. Zucker and S. E. Whitcomb, *Proceedings of the Seventh Marcel Grossman Meeting on Recent Developments in Theoretical and Experimental General Relativity, Gravitation, and Relativistic Field Theories*, Stanford, CA, 24–29 July 1994 (World Scientific, Singapore, 1996).
[4]J. Aasi *et al.*, Class. Quantum Gravity **32**, 115012 (2015).
[5]F. Acernese *et al.*, Class. Quantum Gravity **32**, 024001 (2015).
[6]T. Akutsu *et al.*, Prog. Theor. Exp. Phys. **2021**, 05A101 (2021).
[7]K. Burtnyk, "LIGO-Virgo-KAGRA announce the 200th gravitational wave detection of O4," https://www.ligo.caltech.edu/news/ligo20250320.
[8]M. Evans *et al.*, "A horizon study for Cosmic Explorer: Science, observatories, and community," arXiv:2109.09882 (2021).
[9]ET Steering Committee Editorial Team, "Einstein telescope design report update 2020" (2020).
[10]ET Steering Committee, *ET Cost Book* (ET Steering Committee, 2020).
[11]P. Marin, M. Dialinas, G. Lissillour, A. Marraud, and A. Reboux, Vacuum **49**, 309 (1998).
[12]C. Scarcia, G. Bregliozzi, P. Chiggiato, A. Ingrid Michet, A. T. Perez Fontenla, M. Rimoldi, M. Taborelli, and I. Wevers, J. Vac. Sci. Technol. B **42**, 054202 (2024).
[13]P. Oxley, J. Goodell, and R. Molt, J. Magn. Magn. Mater. **321**, 2107 (2009).
[14]K. J. Hsia, "Brittle-ductile transition," in *Encyclopedia of Tribology* (Springer US, New York, 2013), pp. 273–279.
[15]J. Kamiya, N. Ogiwara, M. Nishikawa, Y. Hikichi, T. Yanagibashi, and M. Kinsho, Vacuum **98**, 12 (2013).
[16]S. Kato, J. Kamiya, K. Yamamoto, M. Yoshimoto, and M. Kinsho, J. Vac. Soc. Jpn. **55**, 160 (2012).
[17]P. Redhead, J. Hobson, and E. Kornelsen, *High Vacuum Series* (Chapman & Hall, London, 1968).
[18]P. Chiggiato, "Outgassing properties of vacuum materials for particle accelerators," arXiv:2006.07124 (2020).
[19]ISO/TS 20177:2018-06: Procedures to measure and report outgassing rates (2018).
[20]Hiden Analytical, TPD workstation, https://www.hidenanalytical.com/products/catalysis-and-thermal-analysis/tdslab-series.
[21]M. Malabaila and L. Ferreira, "Operating procedure for chemical degreasing of parts for high-vacuum and ultra-high-vacuum applications," EDMS No. 1390437 v.3, Technical Report, 2022.
[22]GS-IS & EN-MME, "Stainless steel sheets/plates for vacuum applications," Technical Specification No. 1004—1.4306, EDMS No. 790767, Technical Report, 2013.
[23]H. F. Dylla, D. M. Manos, and P. H. LaMarche, J. Vac. Sci. Technol. A **11**, 2623 (1993).
[24]D. Edwards, Jr., J. Vac. Sci. Technol. **14**, 606 (1977).
[25]K. Kanazawa, J. Vac. Sci. Technol. A **7**, 3361 (1989).
[26]A. Savitzky and M. J. E. Golay, Anal. Chem. **36**, 1627 (1964).
[27]D. M. Grant, D. L. Cummings, and D. A. Blackburn, J. Nucl. Mater. **152**, 139 (1988).
[28]A. N. Itakura, N. Miyauchi, Y. Murase, T. Yakabe, M. Kitajima, and S. Aoyagi, Sci. Rep. **11**, 8553 (2021).
[29]M. R. Louthan and R. G. Derrick, Corros. Sci. **15**, 565 (1975).
[30]R. A. Oriani, Acta Metall. **18**, 147 (1970).
[31]K. L. Wilson and K. L. Baskes, J. Nucl. Mater. **76–77**, 291 (1978).
[32]K. L. Wilson and K. L. Baskes, J. Nucl. Mater. **111–112**, 622 (1982).
[33]M. Bernardini *et al.*, J. Vac. Sci. Technol. A **16**, 188 (1998).
[34]K. Jousten, Vacuum **49**, 359 (1998).
[35]P. Chiggiato, C. Garion, A. T. Perez Fontenla, G. Pigny, C. Scarcia, M. Dakshinamurthy, L. Ferreira, L. Scibile, and M. Taborelli, "ET-pp deliverable 6.2 [vacuum pipe design]" (2024), https://apps.et-gw.eu/tds/ql/?c=17732.